NANO LETTERS

2008
Vol. 8, No. 8
2503-2509

Ligand-Induced Structural Changes in Maltose Binding Proteins Measured by Atomic Force Microscopy

Cristian Staii,*,†,‡ David W. Wood,§ and Giacinto Scoles†,||

Department of Chemistry, Princeton University, Princeton, New Jersey 08544, Department of Chemical Engineering and Department of Molecular Biology, Princeton University, Princeton, New Jersey 08544, and SISSA-ELLETRA Nano Innovation Laboratory, ELETTRA Sincrotrone Trieste Strada Statale 14, 34012 Basovizza, Trieste, Italy

Received May 30, 2008; Revised Manuscript Received June 30, 2008

ABSTRACT

We use atomic force microscopy (AFM) based force-compression measurements to probe the ligand-induced functional conformational changes in surface-immobilized dicysteine-terminated maltose binding proteins (dicys-MBPs). The proteins are immobilized at well-defined locations directly on Au substrates using the previously reported technique of nanografting. By measuring the difference between the ligand-free and ligand-bound mechanical work performed by the AFM-tip during the protein compression, we determine the open−closed transition energy for dicys-MBPs to be $\Delta E_0 = (8 \pm 4)$ Kcal/mol. We also compare the binding kinetics of two different ligands (maltose and maltotriose) to dicys-MBPs by performing AFM-friction measurements. We show that our results are consistent with a simple model for the surface-immobilized dicys-MBPs: the protein consists of two rigid lateral lobes connected by a hinge-loaded spring.

Maltose binding protein (MBP) is a 370 amino acid molecule belonging to the large family of periplasmic binding proteins (PBPs). This is a class of ligand-specific binding proteins that mediate the efficient uptake of nutrients across the inner membrane of gram-negative bacteria, and also serve as sensors for signaling through the chemotaxis system.[1–3] Almost all PBPs share a fundamental two-domain structural fold consisting of two lobes (domains) of similar size linked by a flexible, multistranded "hinge" region, which acts as a binding site for various ligands.[4–6] For MBP this hinge region consists of a short helix and a two-stranded β sheet.[5,7]

MBP binds sugars with micromolar affinity, resulting in a ligand-mediated "open to closed" transition.[4,8,9] This functional conformational change is common to all PBPs, and it involves a reorientation of the two lobes around the hinge region: in the ligand-free ("open") state the position of the two lobes exposes the binding site, whereas in the ligand-bound ("closed") structure, they rotate and fold relative to one another, trapping the ligand in the central binding cleft (Figure 1a).[2,4] The change in the interdomain angle induced by this ligand-binding motion is about 35°, while there is very small relative translation of the two domains.[2,10] This conformational change affects the chemotactic response in *E. coli.* MBP has surface residues on both lobes that contact the receptor protein Tar.[1] In the open state, the two MBP lobes and their corresponding residues are far apart, leading to a low binding affinity of these surface residues to the Tar receptor. In the closed state, the two lobes rotate and twist laterally allowing the surface residues to simultaneously contact the Tar protein.[1,11] This starts a signal transduction process that ultimately influences the motion of the *E. coli* flagella, thereby directing the motion of the bacteria toward nutrients.[12]

Previous work[13–17] has shown that protein patterning on the scale of 100 nm with precise control over pattern position and geometry can be achieved using an atomic force microscope (AFM)-based nanolithography technique called nanografting.[18,19] For example, we have used nanografting to immobilize double cysteine-terminated MBPs (dicys-MBP for short) at well-defined locations directly onto gold substrates. By monitoring the change in the frictional force between the AFM-tip and the nanografted protein patch, we were able to monitor the in situ bioactivity of dicys-MBP and show that the maltose-binding function is maintained upon immobilization.[17]

In addition to our group,[14] several other groups have used externally applied forces as natural variables for probing the free energy surface of biomolecules, from randomly bound surface proteins[20] to nucleic acids and molecular motors[21]

* Corresponding author. E-mail: cstaii@wisc.edu.
† Department of Chemistry, Princeton University.
‡ Current address: Department of Physics, University of Wisconsin, Madison, 1150 University Avenue, Madison, Wisconsin 53706.
§ Department of Chemical Engineering and Department of Molecular Biology, Princeton University.
|| SISSA-ELLETRA Nano Innovation Laboratory.

10.1021/nl801553h CCC: $40.75
Published on Web 07/22/2008

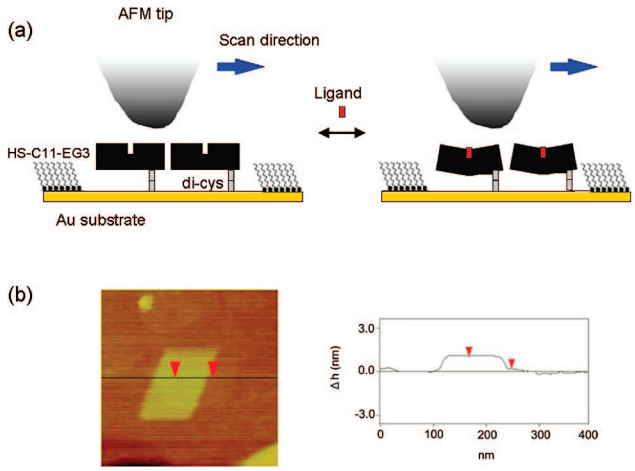

Figure 1. (a) Schematic of MBP with a double-cysteine (dicys) linker nanografted into an undecanethiol triethylene glycol SAM on a Au substrate. The COOH terminus of MBP is used as an attachment site for the dicys linker, orienting the ligand-binding cleft toward the buffer solution. MBP undergoes a conformational change upon introducing various ligands (maltose or maltotriose, for the data shown in this paper) from an "open" (ligand-free) state (left) to a "closed" (ligand-bound) state (right). This ligand induced "hinge-bending motion" can be detected by AFM friction measurements.[17] (b) AFM height image (left) and corresponding line scan for a nanografted dicys-MBP patch.

(for a review, see ref 21). Single molecule force spectroscopy is a very useful technique, but measurements are not trivial, as in this case fluctuations are large and signals are low.[20] The advantages of a multimolecule approach in which all molecules have the same orientation is that, the collective number and mass being larger, fluctuations are smaller and therefore the measurements are easier. Furthermore, a cluster (~1000) of molecules is easier to model theoretically because periodic boundary conditions can be applied in this case as in the case of bulk matter.[22] We also emphasize that many of the advantages of single molecule experiments (lack of ensemble averaging, control over the direction of applied forces[20] etc.) are retained in multimolecule experiments where all molecules are oriented in the same way, as is the case in nanografting (see below).

We have previously demonstrated that (a) our proteins are surface-bound in well-defined nanosize locations, (b) they have a well-controlled orientation, and (c) they preserve their biochemical activity almost as if they were still free in solution.[17] In this paper, we use AFM force-compression measurements to probe the ligand-induced changes in the mechanical properties of dicys-MBP proteins nanografted onto Au surfaces. In addition, we compare the binding kinetics of two different ligands (maltose and maltotriose) to MBP by performing AFM-friction measurements.

The genetically engineered dicys-MBPs, their purification, and the nanografting process have been presented in detail elsewhere.[17,23,24] Briefly, we use standard recombinant DNA techniques to insert two additional cysteine residues to the C-terminus of the *E. coli* maltose binding domain (MBD). The expression and high-throughput purification of the dicysteine terminated MBD is performed using self-cleaving elastin-like polypeptide fusion tags.[23] For immobilizing the proteins at specific locations onto the Au substrate, we use nanografting, an AFM-based nanolithography technique,[14,17–19] consisting of 3 main steps: first a self-assembled monolayer (SAM) of undecanethiol triethylene glycol (HSC_{11}-EG_3) (ProChimia Surfaces Sp., Poland) is deposited onto the Au substrate, and a flat region of this surface is selected by AFM-imaging at low force; second, a small area of the selected region ($\sim 10^4$ nm^2) is scanned at a relatively high load to catalyze the exchange of the HSC_{11}-EG_3 molecules from the original SAM with the cysteine terminated proteins present in the adjacent buffer solution; the result is the formation of a nanografted "protein patch" which can then be visualized in situ at low applied forces via topography measurements with the same AFM tip. Therefore, nanografting allows to immobilize dicys-MBP at well-defined locations directly onto the Au substrate, and to determine the orientation of these proteins via AFM-height measurements. In addition, the whole procedure is carried out in the native protein buffer (containing a small amount of alcohol to facilitate the solubility of the displaced molecules), such that the proteins are very likely to retain their folding conformation and therefore their bioactivity.

As previously described,[17] the inserted double-cysteine linker serves a double role: (a) it provides a unique site for protein immobilization on the substrate, and (b) it ensures that the dicys-MBP molecule has only one possible orientation on the Au substrate upon nanografting (nanografting replaces the sulfur−gold interaction of the original alkanethiol SAM with a sulfur−gold interaction involving the C-terminal cysteine of the protein; see Figure 1b and Figure 6). This arrangement is also designed to orient the ligand-binding site of the nanografted MBP molecules toward the buffer solution (Figure 1a).

Both nanografting and AFM-imaging were performed using a Digital Instruments MultiMode AFM (Santa Barbara, CA) with a Nanoscope IIIa controller. The scanner (Type E, Digital Instruments) was calibrated in the Z direction by measuring atomically resolved gold steps. Experiments were performed in a liquid cell kept at room temperature and placed in an acoustic isolation box (Molecular Imaging, Tempe, AZ). We have used commercially available V-shaped cantilevers with oxide-sharpened Si_3N_4 tips (NP-S Veeco Probes, Camarillo, CA) with a spring constant of 0.58 N/m, and a tip radius of curvature $R_{tip} = 15-20$ nm. The cantilever dimensions reported by the manufacturer are 115 μm (length), 25 μm (width), and 0.6 μm (thickness). The cantilever's Young's modulus is 150 GPa, and the tip height is 3 μm.

Figure 1a shows the schematic of the surface-immobilized proteins and their ligand-induced conformational changes. A typical AFM topographic image of a nanografted dicys-MBP patch is shown in Figure 1b. The measured height of the patch above the HSC_{11}-EG_3 SAM is 1.1 nm, which gives a total height of the dicys-MBP of about 3.4 nm[17] in good agreement with the protein dimensions reported in the literature.[4,6] The rate of successful nanografting attempts for these proteins is about 80%, as reported previously.[17]

We have previously reported[17] that the maltose-mediated conformational change within the dicys-MBP changes the

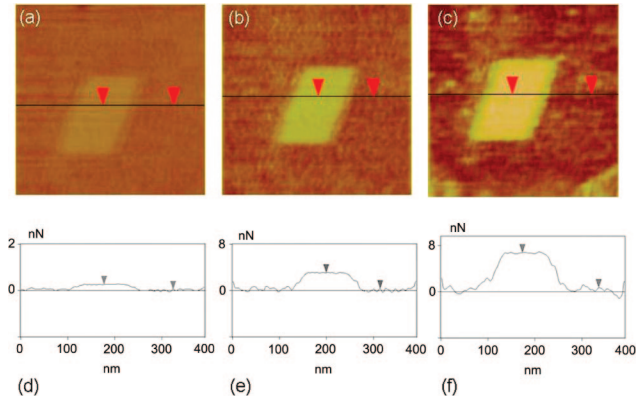

Figure 2. Lateral friction images between the AFM-tip and the nanografted protein patch/SAM substrate for three different maltotriose concentrations: 0 M (a), 50 nM (b), and 100 nM (c). (d−f) Line scans corresponding to the black lines in images a−c.

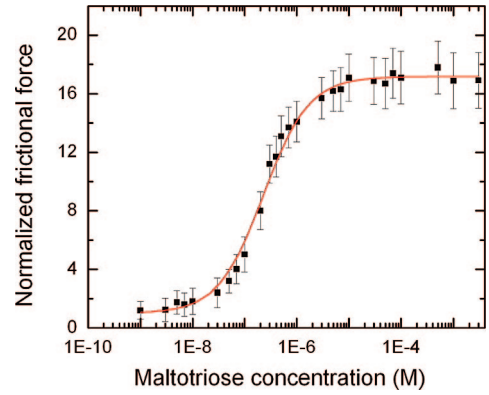

Figure 3. Dependence of the normalized lateral frictional force on maltotriose concentration (squares), and fit to the data with a binding isotherm (solid curve). Error bars represent the rms values of the normalized frictional force measured at each maltotriose concentration.

AFM-tip−protein interaction, therefore causing the frictional signal to change. By measuring the change in the frictional force above the protein nanopatterns as a function of maltose concentration, we have measured the dissociation constant for the dicys-MBP/maltose system: $k_{\mathrm{dmaltose}} = (1 \pm 0.04)\ \mu$M. We have also shown that these surface-confined proteins can be regenerated, and their frictional response is reproducible through several maltose exposure/washing cycles.[17]

We start by comparing these previously reported results on maltose with the binding of another ligand, maltotriose to dicys-MBP, by measuring the change in the frictional force between the AFM-tip and the protein nanopatterns as a function of maltotriose concentration. The experimental conditions are similar to the ones reported in ref 17 for maltose. Figure 2 shows an example of lateral friction images for three maltotriose concentrations: 0 M (Figure 2a), 50 nM (Figure 2b), and 100 nM (Figure 2c), obtained at low (0.5 nN) vertical load. In the absence of maltotriose and with the tip above the SAM matrix, the lateral frictional force (F^0_{sub}) has an average (background) value of (0.1 ± 0.02) nN, while the same force with the tip above the protein patches is $F^0_{\mathrm{patch}} = (0.3 \pm 0.02)$ nN (Figure 2a). Upon changing to a 50 nM maltotriose solution, the values of the two frictional forces change respectively to $F^{\mathrm{M}}_{\mathrm{sub}} = (0.3 \pm 0.05)$ nN (substrate) and $F^{\mathrm{M}}_{\mathrm{patch}} = (2.8 \pm 0.05)$ nN (patch; Figure 2b). For 100 nM maltotriose, the two values become $F^{\mathrm{M}}_{\mathrm{sub}} = (0.5 \pm 0.1)$ nN (substrate) and $F^{\mathrm{M}}_{\mathrm{patch}} = (6.8 \pm 0.1)$ nN (patch; Figure 2c). Thus, the relative change in the lateral frictional force above the patch upon addition of 50 nM of maltotriose is $F^{\mathrm{M}}_{\mathrm{patch}}/F^0_{\mathrm{patch}} = 9.3$; that is approximately 3 times larger than the same change above the SAM matrix ($F^{\mathrm{M}}_{\mathrm{sub}}/F^0_{\mathrm{sub}} = 3$). For 100 nM maltotriose, the friction increase above the patch is 4.5 times larger than the same increase above the substrate ($F^{\mathrm{M}}_{\mathrm{patch}}/F^0_{\mathrm{patch}} = 22.6$, $F^{\mathrm{M}}_{\mathrm{sub}}/F^0_{\mathrm{sub}} = 5$). There is no significant change in the protein height h with maltotriose concentration ($h = 3.4$ nm). This is consistent with the fact that in our configuration (Figure 1) the maltotriose-induced rotation of the two protein lobes takes place in a plane which is approximately parallel to the Au surface, and therefore the protein height is not expected to change noticeably. We also note that after removing the maltotriose by washing the patch with pure buffer for 25 min, the frictional forces are restored to their initial values, showing that the maltotriose-binding is a reversible process. We conclude that the conformational changes of the dicys-MBP protein induced by maltotriose binding events, allows for ligand binding to be detected by AFM-friction experiments. Similar results have been previously reported for maltose-induced conformational changes in dicys-MBP.[17]

In Figure 3, we show the measurement of the specific binding of maltotriose to dicys-MBP. The data show the dependence of the normalized frictional force: $F_{\mathrm{N}} = (F^{\mathrm{M}}_{\mathrm{patch}}/F^0_{\mathrm{patch}}) \cdot (F^0_{\mathrm{sub}}/F^{\mathrm{M}}_{\mathrm{sub}})$ on the maltotriose concentration measured in the range 0−3 mM. By assuming a linear dependence between the frictional force and the fraction of bound maltotriose in a patch,[17] the data can be fitted with a single-site binding isotherm using the plateau response in the amount of binding (maximum normalized frictional force) and the maltotriose dissociation constant $k_{\mathrm{dmaltotriose}}$ as free parameters. The fit gives a value of the dissociation constant for the surface-bound dicys-MBP/maltotriose system: $k_{\mathrm{dmaltotriose}} = (0.22 \pm 0.01)\ \mu$M which is close to the value of 0.16 μM reported in the literature for proteins in solution using both fluorescence[25] and rapid-kinetic techniques.[26] We explain this similarity by the particular orientation of the nanografted dicys-MBPs (Figure 1a), which exposes the binding sites to the buffer solution, and therefore facilitates the ligand binding.

Having compared the binding kinetics of the two different ligands (maltotriose vs maltose), we focus next on force-compression measurements. First, we probe the dicys-MPB/maltose system and measure the response of both maltose-free and maltose-bound ($k_{\mathrm{dmaltose}} = 1 \pm 0.04\ \mu$M)[17] dicys-MBP patches to different externally applied forces (Figure 4). Specifically, we measure the change in the nanografted patch height for different values of the imaging force applied to the AFM-tip. Figure 4 shows the change in protein height plotted versus the imaging force, for the patch shown in Figure 1b. This height change is expressed as $\Delta h = h_{\mathrm{F}} - h_0$, where $h_0 = 2.3$ nm is the SAM height[17] and h_{F} is the protein

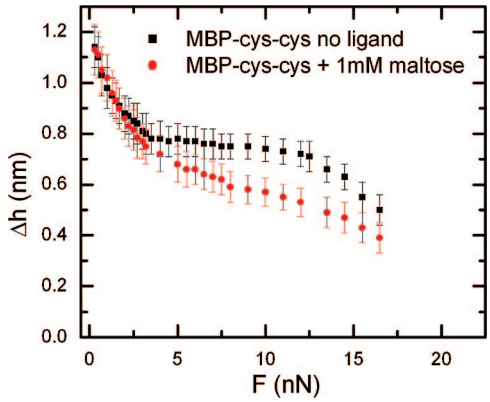

Figure 4. Change in the protein height vs imaging force for a maltose-free (black squares) and maltose-bound (red circles) dicys-MBP protein patch nanografted on Au. The values for height/error at each force represent the average/standard deviation for 20 line scans, similar to the one shown in Figure 1b. The area between the maltose-free and maltose-bound curves is equal to the difference in mechanical work between the two cases. This area divided by the total number of proteins compressed by the tip (see text) gives a difference in mechanical work/protein of (8 ± 4) Kcal/mol, which is close to the measured free energy change due to the open−closed transition.

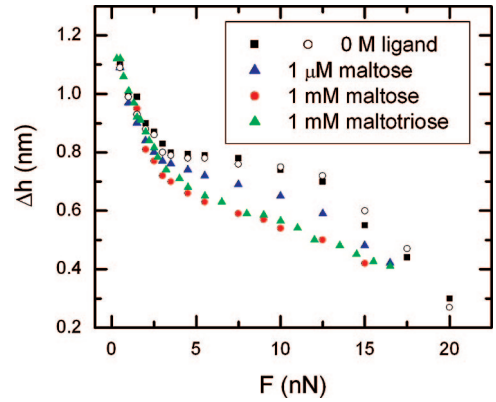

Figure 5. Change in the protein height vs imaging force for a ligand-free (black squares, open circles), maltose-bound (blue triangles, red circles), and maltotriose-bound (green triangles) dicys-MBP protein patch nanografted on Au. The data represented as squares, triangles, and closed (red) circles were obtained by sequentially increasing the imaging force from 0.5 to 17 nN, whereas the open circles are results obtained by gradually decreasing the force from 20 nN to 0.5 nN. The maximum imaging force is 20 nN for maltose-free MBP and 17 nN for ligand-bound MBP. For larger values of the applied force the patch is irreversibly damaged.

height at different imaging forces, varying from 0.5 nN to 17 nN. The data points represented by black squares are obtained by measuring Δh in response to a sequential increase in the imaging force, and in the absence of maltose (maltose-free MBP). The data sets represented by red circles are similar measurements taken for the same dicys-MBP patch after 1 mM of maltose solutions was added to the system (maltose-bound MBP). Figure 4 shows at least two distinct differences between the force response of maltose-free and that of maltose-bound MBP: (a) the same compression is achieved with a higher force for maltose-free MBP than for the maltose-bound protein, and (b) the curves for maltose-free MBP show a plateau response for intermediate forces (3−12 nN), while this plateau is much less pronounced in the data for maltose-bound proteins. Similar results were obtained for two other protein patches (data not shown).

Furthermore, from Figure 4, we have that the difference between the maltose-free and the maltose-bound mechanical work performed by the AFM-tip during the compression is equal to the area between the curves represented by black squares and red circles, which is $(2.2 \pm 0.9) \times 10^{-18}$ J. The estimated size of the contact area between tip and the proteins is (1000 ± 200) nm^2. The MBP lateral dimensions reported by crystallographic studies are 4 × 6.5 nm.[2,4] Therefore, the tip compresses (38 ± 7) protein molecules, and the difference in compression energy (free vs bound) per protein is $\Delta E_0 =$ (8 ± 4) Kcal/mol, a value which is close to the open (ligand-free) to closed (ligand-bound) transition energy measured by either fluorescence spectroscopy ($G_0 = 8.4 \pm 0.2$ Kcal/mol for maltose)[10] or calorimetric measurements ($G_0 = 8.14$ Kcal/mol and $G_0 = 8.34$ Kcal/mol for maltose and maltotriose, respectively).[8]

Figure 5 shows a comparison between different AFM-compression force curves measured for a dicys-MBP patch, for both maltose-bound (1 μM blue triangles, 1 mM red circles) and maltotriose-bound (green triangles) proteins (the data collected in the absence of both maltose and maltotriose is shown as black squares and open circles). For clarity, only the average value for each height is displayed (error bars are at the level indicated in Figure 4, and the height average values are obtained following the procedure described in the caption of Figure 4). The data points represented by black squares and open circles were collected in a time interval of 30 min and in the absence of ligand (maltose, maltotriose). First, Δh is measured in response to a sequential increase in the imaging force between 0.5−20 nN (black squares). Then, the measurements are repeated by rescanning the patch and gradually decreasing the force from its maximum to its minimum values (open circles). The identity of these two compression curves (lack of hysteresis) shows that the compression is reversible and the MBP protein patches are elastic. This result is in contrast with similar measurements done on other proteins such as the 4-helix bundle proteins, where the recovery of the protein original structure was not instantaneous, suggesting that a conformational change was possibly induced by the AFM-tip.[14] Second, the compression curve for 1 μM maltose (blue triangles) falls right in between the maltose-free (black squares) and maltose-bound (1 mM, red circles) curves. We are going to show below that this result is consistent with a measured dissociation constant for maltose of $k_{\mathrm{dmaltose}} = 1$ μM.[17] Finally, Figure 5 shows that the response of the protein molecules to the externally applied forces is almost identical for the two different ligands (maltose and maltotriose) at 1 mM, when all proteins are in the bound state.

Previous experimental[2,6,10,27] and theoretical[7,27] studies have shown that the two MBP domains behave largely like rigid bodies during the reversible open−closed transition, with very little change in the structure within either domain.

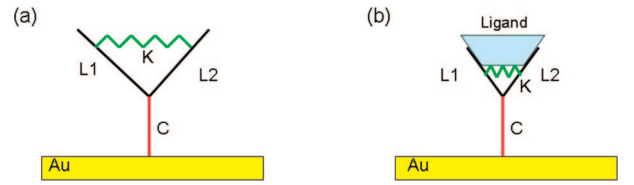

Figure 6. Model of the ligand-free (a) and ligand-bound (b) dicys-MBP protein, immobilized on the Au substrate. The two lateral domains L1, L2 are represented as rigid bodies connected by a "hinge-spring" K. The central ligand binding cleft and the double-cysteine linker are represented as another rigid body C. The central spring K holds the protein open by separating L1 and L2 in the absence of the ligand (a). Ligand binding stabilizes the protein in the closed state by compressing the spring (b).

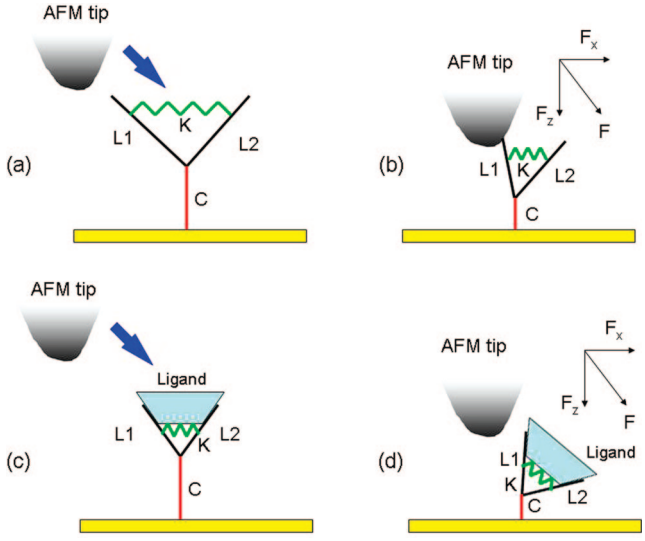

Figure 7. Model for the interaction between the dicys-MBP and the AFM-tip, for both the ligand-free (top) and ligand-bound (bottom) case; (a,b) As the AFM-tip approaches the ligand-free protein from the side (a), it both compresses the protein and moves the two lateral lobes closer (L1, L2) together, by compressing the hinge-loaded spring K (b); (c,d) For the ligand-bound proteins, the two lobes are locked by the ligand (c), and therefore the result of the protein-tip interaction is a rigid rotation of the lobes and an overall compression of the protein (d). No mechanical work is done in this case to compress the central hinge spring K.

Moreover, the MBP flexible central binding cleft behaves as a "spring-loaded hinge" which holds the protein open in the absence of the ligand. The "spring" is the result of several interdomain interactions that minimize the accessible hydrophobic surface area near the hinge in the absence of ligand.[7,10,27] As the protein closes, several well-defined molecular rearrangements take place and a number of residues in the binding cleft are buried, which in turn leads to an increase in the exposed hydrophobic surface area localized in the hinge region. The process can be modeled as a compression of the "hinge spring" which exerts an opening force, which in turn correlates linearly with the closing angle.[10] Upon ligand binding, a salt bridge between a side chain in the hinge region and a residue in the N-terminal domain is formed and it operates as a latch that locks the ligand-bound MBP in the closed configuration.[7] This interaction, together with the favorable protein−sugar hydrogen-bonding forces overcomes the unfavorable energetics of compressing the "hinge spring".

Based on the results summarized in the previous paragraph, we propose the following simplified model of the dicys-MBP nanografted onto Au (Figure 6): the protein consists of two rigid lobes (L1, L2) connected by a spring (K), and a hinge region immobilized on the substrate via a double-cysteine residue (C). In the open (ligand-free) state, the two lobes are kept apart by the spring K (Figure 6a), while in the closed (bound) state, the new ligand−protein interactions stabilize the protein by overcoming the energetic costs of compressing the spring (Figure 6b).

This simple model explains all of the compression data presented above and can be supported by a systematic examination of the results. First, we focus on the ligand-free case (Figure 6a and 7a). Since the AFM-tip is both scanning laterally and compressing the protein patch, the total applied force has two components: a lateral "scanning component" F_x, parallel to the Au surface, and a "compression component" F_z oriented perpendicular to the surface (Figure 7a,b). Consequently, the total mechanical work done by the tip: $W_{total}^{free} = \int F \cdot dl$ can be separated into two components: (a) the work necessary to compress the protein in the z direction: $W_{comp} = \int F_z \cdot dh$, and (b) the spring-compression work: $W_{spring} = \int F_x \cdot dx$, such that

$$W_{total}^{free} = \int F_z \cdot dh + \int F_x \cdot dx \qquad (1)$$

At relatively low force loads, both protein lobes are simultaneously tilted while the whole protein is compressed by the AFM-tip. At intermediate forces, when the overall tilt/compression reaches a threshold value, the AFM-tip starts to compress the central hinge-loaded spring K and to close the protein by moving the two lobes closer together (Figure 7b). The total force F applied by the AFM-tip increases during this closure process, but the protein height remains constant since only the lateral force component F_x contributes to the work necessary to compress the spring K. This model is consistent with the ligand-free data shown in Figures 4 and 5, where the curves represented by squares show a plateau of constant Δh at intermediate forces: 3−12 nN. In this intermediate force regime, the AFM-tip induces the open−closed transition of the proteins, with all of the proteins being in the closed state (spring K fully compressed) for $F \approx 12$ nN. At even higher forces, the tip continues the overall compression of the proteins (the 2 lobes are now in close contact and are moved together rigidly) until the patch is irreversibly damaged for $F > 20$ nN (Figure 5).

The process of ligand binding induces an open−closed conformational change, and the transition energy reported in literature[8,10] for this process is $G_0 = 8.4$ Kcal/mol or 5.8×10^{-20} J/protein. During this transition, the relative displacement of the two lobes is $\Delta x = 7$ Å.[28] By using these values, the model shown in Figures 6 and 7 predicts that the spring-loaded hinge has a spring constant:

$$k = 2G_0/\Delta x^2 \approx 0.24 \text{ N/m} \qquad (2)$$

This spring constant can also be calculated from the maltose-free compression data shown in Figures 4 and 5.

Assuming that all of the (38 ± 7) proteins which are simultaneously compressed by the AFM-tip (see above) undergo a tip-induced open−closed conformational change in the intermediate force regime (constant Δh, $\Delta F \approx 9$ nN; see Figure 4), we have that:

$$k = (1/38) \cdot \Delta F/\Delta x = 0.33 \pm 0.06 \text{ N/m} \quad (3)$$

in good agreement with the result (eq 2) obtained from the estimate based on the reported transition energy.

We now consider the force compression data for the ligand-bound case (Figure 7c,d). Here, the two lobes are locked in place by the ligand such that there is no relative motion between them. The spring K is already compressed, and the energetic cost of closing the protein is overcome by the new protein−ligand interactions.[7] The result of the force exerted by the tip is a rigid rotation of the lobes and an overall compression of the protein (Figure 7d). It follows that the protein height decreases monotonically with increasing applied force, and no plateau region is observed in the F versus Δh data, in agreement with the ligand-bound curves presented in Figure 4 and Figure 5. The total mechanical work done by the tip in this case is

$$W_{total}^{bound} = \int F_z \cdot dh \quad (4)$$

From eq 1 and eq 4, we have that the difference in the total mechanical work performed by the AFM-tip in the ligand-bound and ligand-free cases, respectively, is equal to the work done to compress the central spring-loaded hinge K, which in turns equals the open−closed (or ligand-free to ligand-bound) transition energy:

$$\Delta W = W_{total}^{free} - W_{total}^{bound} = \int F_x \cdot dx = G_0 \quad (5)$$

This conclusion is indeed supported by the data presented in Figure 4: the measured area between the ligand-free and ligand-bound curves, equal to the difference in the total mechanical work for the two cases is $(2.2 \pm 0.9) \times 10^{-18}$ J. For the estimated total number of (38 ± 7) proteins simultaneously compressed by the tip, this gives $\Delta W = (8 \pm 4)$ Kcal/mol in extremely good agreement with the transition energy reported in literature.[8,10] Furthermore, although the binding kinetics of maltose and maltotriose to MBP are different, the corresponding transition energies are very similar[8] suggesting that there is a common closed state for both ligands. This is also supported by our data. By fitting the normalized friction versus concentration data for maltotriose shown in Figure 3 with a binding isotherm, we find an equilibrium dissociation constant, $k_{\text{dmaltotriose}} = (0.22 \pm 0.01)$ μM, which is different from what we have previously reported on similar measurements done for maltose: $k_{\text{dmaltose}} = (1 \pm 0.04)$ μM.[17] Moreover, Figure 5 shows that the force-compression curves for maltose (red circles) and maltotriose (green triangles) are very similar, and the same transition energy $\Delta W = (8 \pm 4)$ Kcal/mol is obtained in both cases.

Finally, we note that the measured equilibrium dissociation constant for maltose ($k_{\text{dmaltose}} \sim 1$ μM) implies that at a maltose concentration of 1 μM approximately half of the dicys-MBP proteins are in the ligand-bound state and the other half are in the ligand-free state.[29] Figure 5 shows that the corresponding force compression curve (1 μM maltose) falls right in between the maltose-free (0 M) and the maltose-bound (1 M) force curves. The difference in mechanical work between this intermediate case and the maltose-free compression is about 1/2 of the corresponding difference found for the maltose-bound case, which shows that indeed only approximately half of the ~38 proteins compressed by the tip are in the bound state.

In conclusion, we have used AFM force-compression measurements to probe the ligand-induced changes in the mechanical properties of dicys-MBP proteins nanografted onto Au surfaces. We have reported a new approach for finding the open-closed transition energy in periplasmic binding proteins, based upon measuring the mechanical work performed by the AFM-tip during the protein compression. The values for the transition energy measured using this method are in close agreement with those reported in literature from spectroscopy and calorimetric experiments. These experimental results are explained by modeling the central region of the protein as two rigid lobes connected by a hinge-loaded spring. We have also used AFM-friction measurements to compare the binding kinetics of two different ligands (maltose and maltotriose) to MBP. We found different equilibrium dissociation constants and similar transition energies for the two ligands, consistent with different binding kinetics and a common closed state for both maltose and maltotriose.

Acknowledgment. We thank Professor Gang-yu Liu (UC-Davis), Dr. Nuri Oncel, and Professor Jannette Carey (Princeton University) for useful discussions. This work was supported in part by an Institute for Complex Adaptive Matter (ICAM) postdoctoral fellowship (C.S.), in part by the National Science Foundation (NSF) funded Princeton MRSEC group grant, and in part by a grant from the U.S. Department of Energy (340-6007).

References

(1) Zhang, Y.; Gardina, P. J.; Kuebler, A. S.; Kang, H. S.; Christopher, J. A.; Manson, M. D. *Proc. Natl. Acad. Sci. U.S.A.* **1999**, *96*, 939–944.
(2) Sharff, A. J.; Rodseth, L. E.; Spurlino, J. C.; Quiocho, F. A. *Biochemistry* **1992**, *31*, 10657–10663.
(3) Mowbray, S. L.; Sandgren, M. O. *J. Struct. Biol.* **1998**, *124*, 257–275.
(4) Medintz, I. L.; Deschamps, J. R. *Curr. Opin. Biotechnol.* **2006**, *17*, 17–27.
(5) Fukami-Kobayashi, K.; Tateno, Y.; Nishikawa, K. *J. Mol. Biol.* **1999**, *286*, 279–290.
(6) Spurlino, J. C.; Lu, G. Y.; Quiocho, F. A. *J. Biol. Chem.* **1991**, *266*, 5202–5219.
(7) Stockner, T.; Vogel, H. J.; Tieleman, D. P. *Biophys. J.* **2005**, *89*, 3362–3371.
(8) Thomson, J.; Liu, Y.; Sturtevant, J. M.; Quiocho, F. A. *Biophys. Chem.* **1998**, *70*, 101–108.
(9) Sandros, M. G.; Gao, D.; Benson, D. E. *J. Am. Chem. Soc.* **2005**, *127*, 12198–12199.
(10) Millet, O.; Hudson, R. P.; Kay, L. E. *Proc. Natl. Acad. Sci. U.S.A.* **2003**, *100*, 12700–12705.
(11) Gardina, P.; Conway, C.; Kossman, M.; Manson, M. *J. Bacteriol.* **1992**, *174*, 1528–1536.
(12) Koiwai, O.; Hayashi, H. *J. Biochem. (Tokyo)* **1979**, *86*, 27–34.
(13) Case, M. A.; McLendon, G.; Hu, Y.; Vanderlick, T. K.; Scoles, G. *Nano Lett.* **2003**, *3*, 425–429.
(14) Hu, Y.; Das, A.; Hecht, M. H.; Scoles, G. *Langmuir* **2005**, *21*, 9103–9109.

(15) Liu, G. Y.; Amro, N. A. *Proc. Natl. Acad. Sci. U.S.A.* **2002**, *99*, 5165–5170.
(16) Wadu-Mesthrige, K.; Amro, N. A.; Garno, J. C.; Xu, S.; Liu, G. *Biophys. J.* **2001**, *80*, 1891–1899.
(17) Staii, C.; Wood, D. W.; Scoles, G. *J. Am. Chem. Soc.* **2008**, *130*, 640–646.
(18) Liu, G. Y.; Xu, S.; Qian, Y. *Acc. Chem. Res.* **2000**, *33*, 457–466.
(19) Liu, M.; Amro, N. A.; Liu, G. Y. *Annu. Rev. Phys. Chem.* **2008**, *59*, 367–386.
(20) Brujic, J; Hermans, R. I.; Walther, K. A.; Fernandez, J. M. *Nat. Phys.* **2006**, *2*, 282–284.
(21) Bustamante, C.; Chemla, Y. R.; Forde, N. R.; Izhaky, D. *Annu. Rev. Biochem.* **2004**, *73*, 705–748.
(22) Cheung, M. S.; Klimov, D.; Thirumalai, D. *Proc. Natl. Acad. Sci. U.S.A.* **2005**, *102*, 4753–4758.
(23) Banki, M. R.; Feng, L.; Wood, D. W. *Nature Methods* **2005**, *2*, 659–661.
(24) Banki, M. R.; Wood, D. W *Microb. Cell. Fact.* **2005**, *4*, 32.
(25) Szmelcman, S.; Schwartz, M.; Silhavy, T. J.; Boos, W. *Eur. J. Biochem.* **1976**, *65*, 13–19.
(26) Quiocho, F. A.; Spurlino, J. C.; Rodseth, L. E. *Structure* **1997**, *5*, 997–1015.
(27) Shilton, B. H.; Flocco, M. M.; Nilsson, M.; Mowbray, S. L. *J. Mol. Biol.* **1996**, *264*, 350–363.
(28) Fehr, M.; Ehrhardt, D. W.; Lalonde, S.; Frommer, W. B. *Curr. Opin. Plant Biol.* **2004**, *7*, 345–351.
(29) See, for example, http://www.graphpad.com/curvefit/how_to_derive.htm#example_model_3_equilibrium_binding.

NL801553H